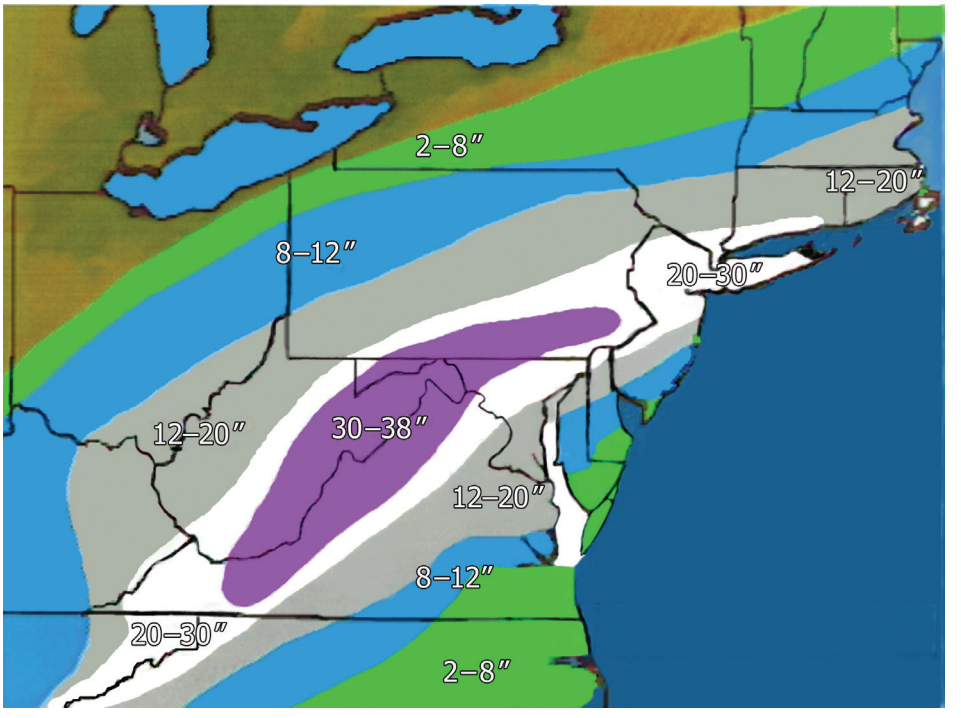

Figure 1.4 Snow depth map from January 6–8, 1996 associated with the "Blizzard of 1996," centered over the middle Atlantic United States (after WRC-TV/NBC 4, Washington, DC analysis).

Figure 1.5 Transportation department snow blower at work clearing Highway 143 between Cedar Breaks and Panguitch, Utah in 2005. (Courtesy R. Julander.)

Figure 1.7 Instrumentation at the Central Sierra Snow Laboratory in Soda Springs, California. (Courtesy R. Osterhuber.)

Figure 1.9 Site of the 239 km^2 Reynolds Creek Experimental Watershed in the Owyhee Mountains about 80 km southwest of Boise, Idaho, operated by the Agriculture Research Service. (Courtesy USDA, Agriculture Research Service; www.ars.usda.gov/is/graphics/photos/.)

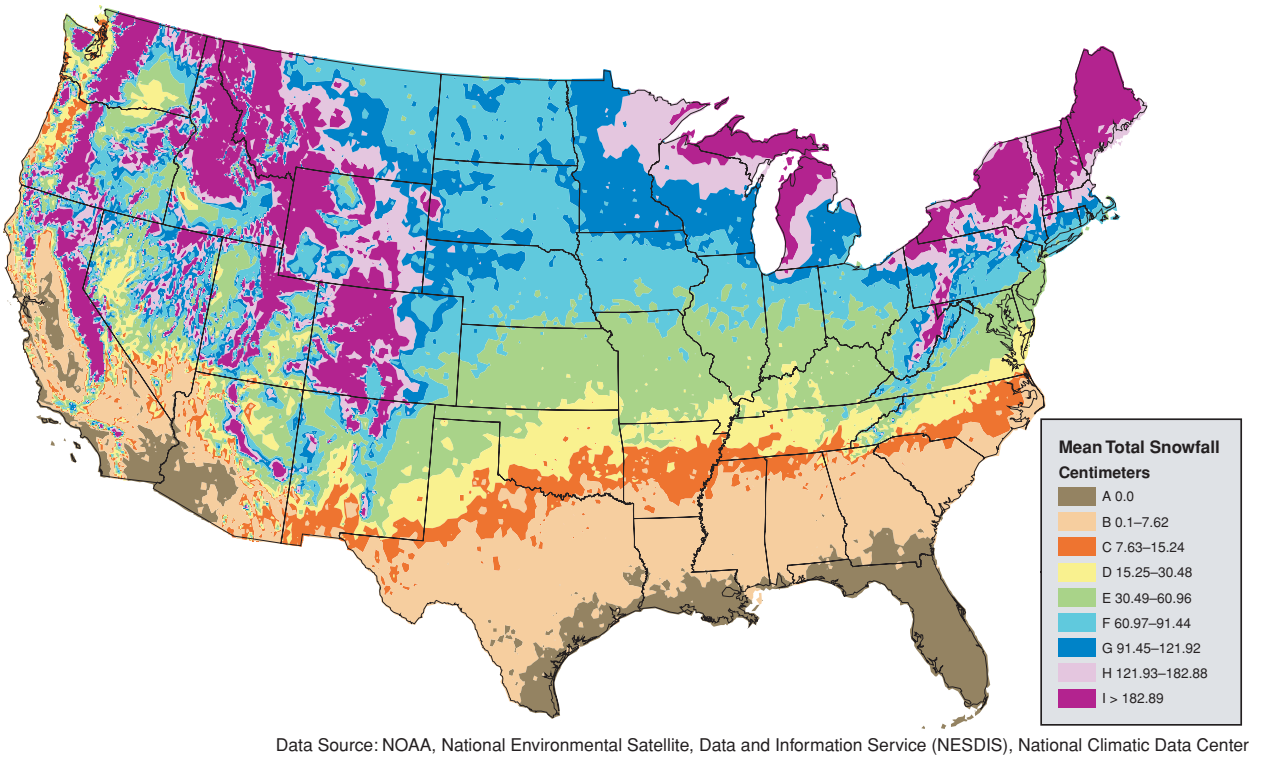

Data Source: NOAA, National Environmental Satellite, Data and Information Service (NESDIS), National Climatic Data Center

Figure 2.6 Mean annual snowfall in the continental United States (modified from USDC, NOAA, National Climate Data Center, Climate Maps of the United States).

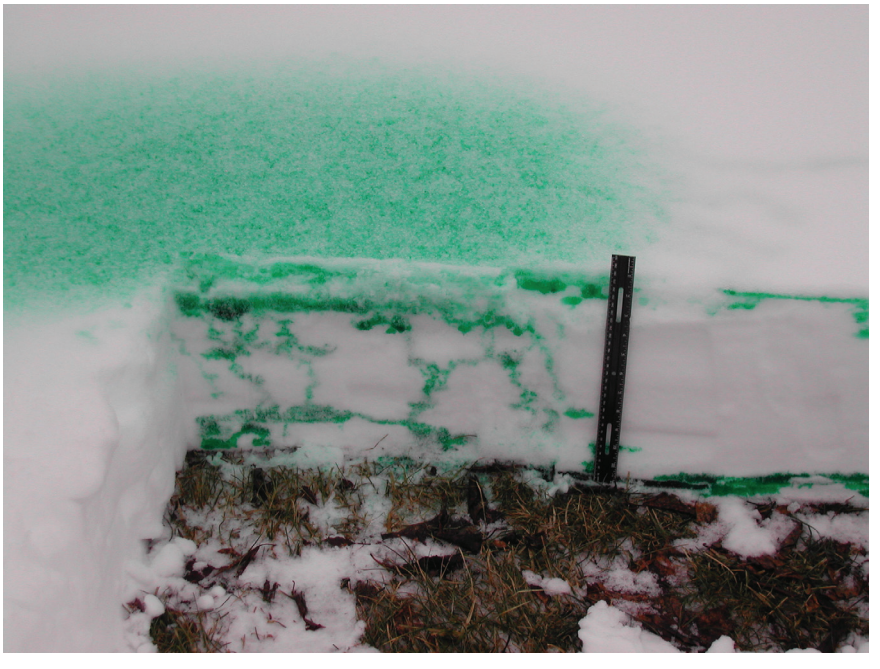

Figure 3.13 Flow fingers for preferential liquid-water movement that formed during initial day's melting of a homogeneous 28-cm depth snowpack resulting from a single snowfall in Pennsylvania (photo D. R. DeWalle). Water mixed with food coloring was uniformly sprayed over the snowpack surface to trace water movement. Also note evidence of meltwater movement downslope to the right in the surface layer and at the soil–snow interface.

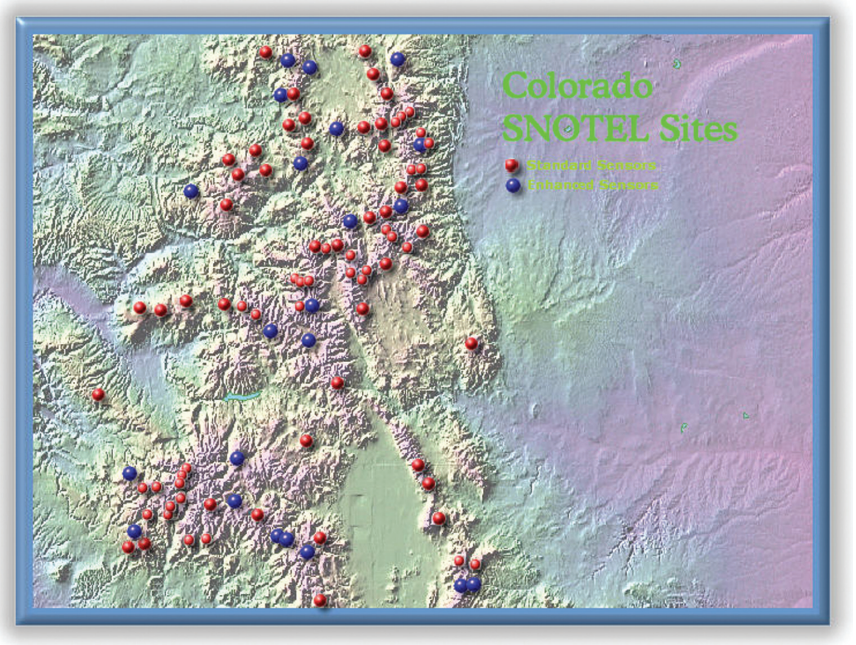

Figure 4.9 Colorado SNOTEL sites (courtesy Natural Resources Conservation Service, US Department of Agriculture).

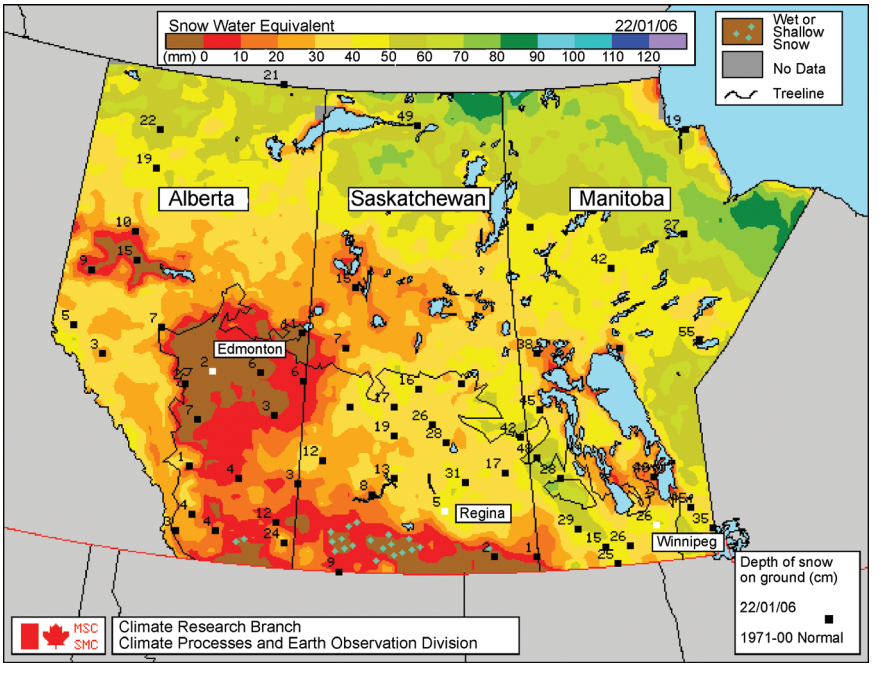

Figure 5.3 Operational snow-water-equivalent map for the Canadian Prairies on January 22, 2006 derived from passive-microwave satellite data. Numbers on the map indicate point measurements of observed snow depth. Maps are distributed by posting on the World Wide Web, www.socc.ca/SWE/snow˙swe.html/. (Reproduced with the permission of the Minister of Public Works and Government Services Canada, 2006.)

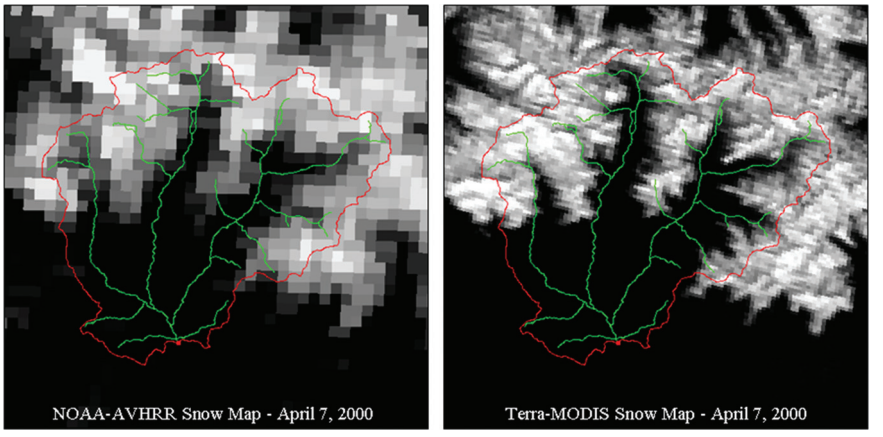

Figure 5.4 Comparison of NOAA-AVHRR and MODIS derived snow cover for the Noguera Ribagorzana Basin (572.9 km^2) in the Central Pyrenees of Spain on April 7, 2000. The different gray levels correspond to different percents of snow cover in each pixel. Snow cover in the Basin totals 181 km^2 from AVHRR and 184 km^2 from MODIS as reported by Rango *et al.* (2003).

Figure 6.1 Radiation instruments at the Penn State, Pennsylvania SURFRAD Network site: (a) pyranometer used to measure incoming shortwave radiation on a horizontal surface, (b) a continuously shaded pyranometer (near) and pyrgeometer (far) used to measure incoming diffuse shortwave and incoming longwave radiation, respectively, (c) tubular pyrheliometer (see arrow) mounted on a solar tracker to measure direct-beam solar radiation at normal incidence, and (d) inverted pyranometer and pyrgeometer on tower to measure reflected shortwave and outgoing longwave radiation from the ground surface (photographs by D. DeWalle).

Figure 6.5 Solar-powered climate stations equipped with data loggers (left) are used to provide data (wind speed, air temperature, humidity) to support computations of snowpack convective exchange. The addition to climate stations of sonic anemometers (top right), fine-wire thermocouples, and high-speed open-path gas analyzers for CO_2 and water vapor (bottom right) allows computation of convective exchange using the eddy covariance method (photographs by D. DeWalle).

Figure 7.4 Prediction of snowmelt in forests requires accounting for canopy effects on snowpack energy exchange, especially radiation exchange. Shadow patterns suggest varying patterns of canopy shading between coniferous forests with foliage (top) and deciduous forests without foliage (bottom) in these pictures from mid-latitude Pennsylvania, USA sites.

Figure 9.4 Rapid delivery of meltwater as overland flow on frozen ground in a pasture swale that has turned the snow into a slush layer.

Figure 12.10 Urban snow requires dedicated areas for snow storage (left) and may lead to accumulation of surface contaminants later in the spring (right) (photos by D. R. DeWalle).

Figure 12.11 Ratnik low-energy modified snow gun (left) and modified fan-type Lenko snow gun (right) being used to augment snowpack for skiing (courtesy of Ratnik Industries, Inc. and Lenko Quality Snow, Inc., respectively).

Figure 12.12 Large slab avalanche in Colorado, USA that began in the alpine startup zone (photo courtesy of Richard Armstrong, US National Snow and Ice Data Center, Boulder, CO).